

Magnetic properties of the half-metallic Heusler alloys Co₂VAl and Co₂VGa under pressure

T. Kanomata,* Y. Chieda, K. Endo, and H. Okada
Faculty of Engineering, Tohoku Gakuin University, Tagajo 985-8537, Japan

M. Nagasako, K. Kobayashi, and R. Kainuma
Department of Materials Science, Graduate School of Engineering, Tohoku University, Sendai 980-8579, Japan

R. Y. Umetsu
Institute for Materials Research, Tohoku University, Sendai 980-8577, Japan

H. Takahashi
Department of Physics, College of Humanities and Sciences, Nihon University, Tokyo 156-8550, Japan

Y. Furutani and H. Nishihara
Faculty of Science and Technology, Ryukoku University, Otsu 520-2194, Japan

K. Abe, Y. Miura, and M. Shirai
Research Institute of Electrical Communication (RIEC), Center for Spintronics Integration Systems (CSIS), Tohoku University, Sendai 980-8577, Japan

(Received 28 June 2010; published 7 October 2010)

Magnetization measurements have been carried out at high pressure up to 12.1 kbar for Co₂VAl and Co₂VGa with a miniature high-pressure clamp cell. The magnetic moment measured at 5 K is independent of pressure for Co₂VGa. This is an experimental observation that gives clear evidence that Co₂VGa possesses half-metallic electronic structure. On the other hand, a sizable pressure dependence of the magnetic moment is observed for Co₂VAl and it is attributed to the precipitation of the bcc particles in the matrix *L*₂₁ phase. The Curie temperature decreases with increasing pressure for Co₂VGa, reflecting characteristics typical for usual itinerant electron systems. The negative pressure dependence of the Curie temperature found in Co₂VGa contrasts fairly with that of other Heusler alloys containing Mn atoms.

DOI: [10.1103/PhysRevB.82.144415](https://doi.org/10.1103/PhysRevB.82.144415)

PACS number(s): 62.50.-p, 71.20.Be, 75.30.Cr

I. INTRODUCTION

Full Heusler alloys are usually defined as ternary intermetallic ordered alloys formed at a stoichiometric composition *X*₂*YZ* with the cubic *L*₂₁ structure, where *X* is any element which belongs to the end of the 3*d*, 4*d*, or 5*d* series, *Y* is a transition-metal element, while *Z* is an *sp* element. The Heusler alloys have been attracting growing interests because of their potential use as half-metallic ferromagnets (HMFs),¹ ferromagnetic shape memory alloys,² and magnetocaloric materials.³ Particularly, the HMFs with the *L*₂₁ structure are expected to be promising materials for device applications in spintronics, for example, tunneling magnetoresistance devices.

Mn-based Heusler alloys *X*₂Mn*Z* show a variety of magnetic properties. The pressure effect on the Curie temperature *T*_C of the ferromagnetic Heusler alloys was studied intensively for Ni₂Mn*Z* (*Z*=Ga, In, Sn, and Sb), Au₂MnAl, Cu₂MnAl, and Rh₂Mn*Z* (*Z*=Sn and Sb),^{4–10} in which Mn atom has the localized moment of about 4 μ_B. For all of the ferromagnetic Heusler alloys *X*₂Mn*Z* mentioned above, *T*_C increases linearly with increasing pressure below about 10 kbar. On the basis of the experimental results, the dependence of the exchange interactions on the interatomic distance was discussed qualitatively for a number of the ferromagnetic Heusler alloys *X*₂Mn*Z*.^{4,5} Recently, Şaşıoğlu *et al.*¹¹ studied theoretically the pressure dependence of *T*_C in

the ferromagnetic Ni₂MnSn by a first-principles density-functional calculation. The calculated pressure dependence of *T*_C in the broad pressure interval is in good agreement with the experimental results.⁸

On the other hand, there has been only a little amount of information about the magnetovolume effect on the Heusler alloys Co₂*YZ* with a high spin polarization. Recently, several authors calculated the electronic structures of Co₂VAl and Co₂VGa.^{12–17} According to the theoretical results, both Heusler alloys Co₂VAl and Co₂VGa are the HMFs with 100% spin polarization.^{13–16} The total magnetic moment should be independent of pressure for HMFs unless 100% spin polarization is degraded by broadening of valence and/or conduction bands with increasing pressure. However, it has not been confirmed experimentally by magnetic measurements under high pressure so far. In this paper, the magnetic properties of Co₂VAl and Co₂VGa under pressure are examined experimentally and theoretically to gain deeper insight into the electronic structure of these materials.

II. EXPERIMENTAL

The polycrystalline alloys Co₂VAl and Co₂VGa were prepared by levitation melting of appropriate quantities of the constituent elements of high purity in an argon atmosphere. The reaction products of Co₂VAl and Co₂VGa were sealed

in the evacuated silica tube, annealed at 1200 °C and 1100 °C for 3 days, respectively, and then quenched into water. To achieve high-crystalline perfection, the reaction products of Co₂VAl and Co₂VGa were subsequently annealed at 600 °C for 7 days and finally quenched into water. The phase identification and characterization of the samples were carried out by x-ray powder diffraction measurements using Cu *K*α radiation. To relieve internal strains in the powder samples, the samples were heated at 600 °C for 2 h.

The thin-film specimens for transmission electron microscopic (TEM) observation were prepared by double jet electropolishing with a solution composed of 8% perchloric acid, 72% acetic acid, 12% ethanol, and 8% ethylene glycol at room temperature. Conventional and high-resolution TEM (HRTEM) observations were carried out by JEM-2000EXII and JEM-2100, respectively, at an acceleration voltage of 200 kV.

The T_C at high pressure was determined by an ac transformer method. The primary and secondary coils were wound on the sample rod with about 1 mm in diameter. An ac current of a constant amplitude flowed in the primary coil and the second voltage, which is directly proportional to initial permeability μ , was recorded as a function of temperature at various pressures. The amplitude and the frequency of the ac magnetic field to the sample are about 7 Oe and 1 kHz, respectively. Hydrostatic pressure was applied to a sample in a Teflon pressure sample cell filled with a liquid pressure-transmitting medium (Fluorinert) by using a piston-cylinder-type device. In this Teflon cell, a sample was placed in a cylindrical cell made of BN with high thermal conductivity. The temperature was measured with a chromel-alumel thermocouple, kept in contact with the sample. The applied pressure was calibrated by using the Hg solid-liquid transition temperature. The T_C at ambient pressure was determined by the ac transformer method as well as the case of the permeability measurements under pressure though we used the different permeability measurement apparatus.

The magnetization measurements at high pressure up to 12.1 kbar were performed using a superconducting quantum interference device magnetometer and a piston-cylinder-type pressure cell made by CuBe alloy. The applied pressure was estimated from the superconducting critical temperature using a tin manometer. The sample and the tin manometer were compressed in a Teflon capsule filled with a liquid pressure-transmitting medium (Daphne 7373). The magnetization M_{cell} arising from the pressure cell with the Teflon capsule, the pressure-transmitting medium, and tin manometer was estimated from the difference between the magnetization at 5 K with and without the pressure cell. All the magnetization data were corrected by subtracting M_{cell} .

III. RESULTS AND DISCUSSION

A. Crystal structure and microstructure

The structural refinement of Co₂VAl and Co₂VGa were performed by the x-ray powder diffraction data using the standard Rietveld technique. Figures 1(a) and 1(b) show the experimental and calculated x-ray powder diffraction patterns for Co₂VGa, respectively. The pattern of Fig. 1(b) was

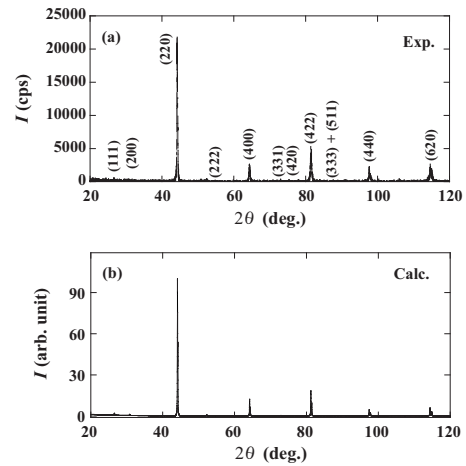


FIG. 1. The x-ray powder diffraction patterns obtained for Co₂VGa; (a) experimental and (b) calculated data.

calculated as the $L2_1$ structure with a space group $Fm\bar{3}m$ in which A (0, 0, 0) and C (1/2, 1/2, 1/2) sites are occupied by Co atoms, and B (1/4, 1/4, 1/4) and D (3/4, 3/4, 3/4) sites occupied by V and Ga atoms, respectively. As seen in Figs. 1(a) and 1(b), the Co₂VGa specimen seems to have a single-phase structure based on the bcc structure. Although a faint (111)_{L21} reflection typifying the $L2_1$ bcc-ordered structure can be detected, no quantitative analysis on the degree on order of the $L2_1$ structure is possible for the experimental result because of the low intensity of the ordered reflections. Very recently, Umetsu *et al.*¹⁸ have investigated the atomic configuration of the Co₂VGa alloy powder annealed at 873 K by using neutron diffraction and confirmed that the Co₂VGa alloy possesses a single-phase structure with an almost perfect $L2_1$ structure. The lattice parameter of Co₂VGa was found to be 5.7920 Å, which is in good accordance with the value reported earlier.¹⁹

Figures 2(a) and 2(b) show the experimental and calculated x-ray powder diffraction patterns for Co₂VAl, respectively. The pattern of Fig. 2(b) was calculated as the $L2_1$ structure. As seen in Fig. 2(a), the faint superlattice reflec-

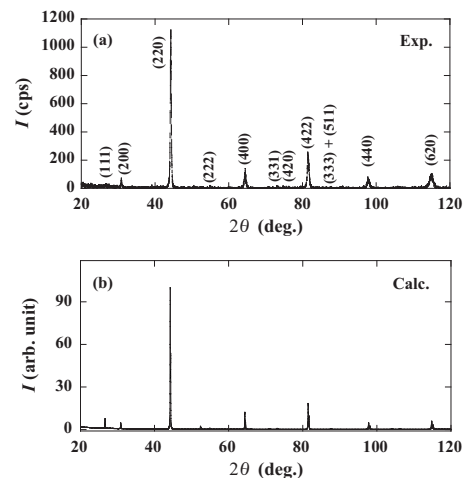


FIG. 2. The x-ray powder diffraction patterns obtained for Co₂VAl; (a) experimental and (b) calculated data.

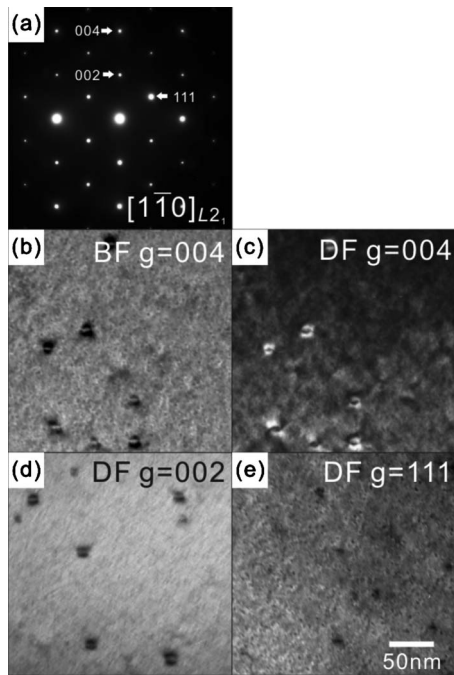


FIG. 3. SADP and TEM BF and DF images under two-beam conditions near $[1\bar{1}0]$ axis for Co_2VAl ; (a) SADP, (b) BF $g=004$, (c) DF $g=004$, (d) DF $g=002$, and (e) DF $g=111$.

tions $(111)_{L21}$ and $(200)_{L21}$ are detected and the Co_2VAl specimen also seems to have a single-phase structure with the ordered $L2_1$ whose lattice parameter was evaluated as being 5.7798 Å. However, the relative intensity of the $(111)_{L21}$ to the $(200)_{L21}$ in the experimental pattern [Fig. 2(a)] is too small in comparison to that in the calculated pattern [Fig. 2(b)]. For such a discrepancy between the experimental and the calculated patterns, there are two possible explanations, i.e., due to decrease in the degree on order of the $L2_1$ structure and due to phase separation between the $L2_1$ phase and another bcc phase. The previous case corresponds to the condition that an atomic interchange occurs between V and Al sites, which has already been pointed out by Ziebeck and Webster¹⁹ and Shreder *et al.*²⁰ The latter case is expected by precipitation of the A2 or B2 phase with the same bcc structure as the $L2_1$ matrix phase and the similar behavior has been reported in Co_2CrAl alloy.²¹ In order to decide the origin of the discrepancy between the experimental and calculated patterns, TEM observations were carried out.

Figures 3(a)–3(e) show the selected area electron diffraction pattern (SADP) near $[1\bar{1}0]_{L21}$ axis and the bright-field (BF) and dark-field (DF) images taken under two-beam conditions from the Co_2VAl specimen, where (b) and (c) are the BF and DF images from $g=004$, and (d) and (e) are the DF images from $g=002$ and $g=111$, respectively. Including both the $(002)_{L21}$ and $(111)_{L21}$ spots, the SADP exhibits a typical pattern of the Heusler $L2_1$ structure, which is consistent with the result by the x-ray diffraction (XRD) examination. The matrix phase shows bright contrast in all the DF images, which means that the matrix has the $L2_1$ structure. As shown in the BF image of Fig. 3(b), however, two types of particles,

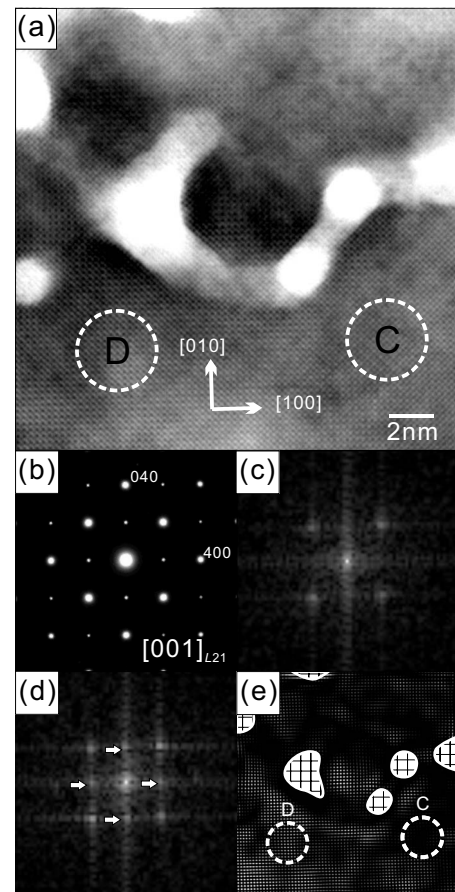


FIG. 4. HRTEM lattice image and corresponding SADP in $[001]$ axis for Co_2VAl ; (a) lattice image and (b) SADP, where (c) and (d) are FFT power spectra taken from regions C and D in (a), respectively, and (e) is RFFT image of (a) constructed from $\{200\}_{L21}$ superlattice spots indicated with four white arrows in (d). The hatched regions in (e) correspond to the holes of thin film in (a).

i.e., large particles with dark contrast of around 20 nm like coffee beans and very small spherical particles with gray contrast of several nanometer are observed. The larger particles in the DF images from both $g=002$ and $g=111$ exhibit a dark contrast similar to those in the BF image from $g=004$ while showing a bright contrast in the DF image of $g=004$. These mean that the larger particle has a disordered bcc structure. On the other hand, although apparently detected in the DF image from $g=111$, the dark contrasts corresponding to the smaller particles are not clear in that from $g=002$. From these results, the smaller particles are considered to possess the disordered bcc structure or a B2-type structure. Figures 4(a) and 4(b) show the lattice image and its corresponding SADP in $[001]_{L21}$ axis taken from the Co_2VAl specimen, respectively. Whereas the lattice fringes basically continue in the observed whole area, inhomogeneous dark contrasts with size of several nanometer are observed and in the edge region of the thin foil, some holes are detected as shown in Fig. 4(a). Although the origin of the formation of holes is not clear, this behavior suggests that some chemical inhomogeneity exists in the specimen at least. From the lattice image, two kinds of fast Fourier transformation (FFT) power spectra can be obtained as shown in Figs. 4(c) and

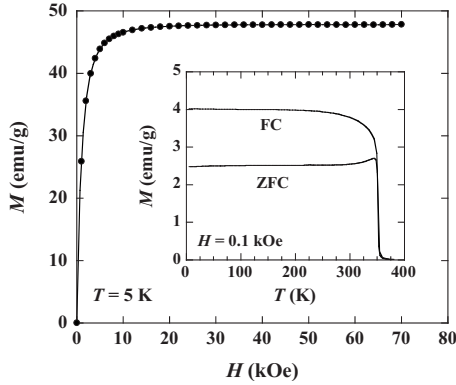


FIG. 5. Magnetization curve measured at 5 K for Co_2VGa . The inset shows the temperature dependence of the magnetization M at 0.1 kOe for the ZFC and the FC processes.

4(d), which were taken from the areas C and D in Fig. 4(a), respectively. Here, the pattern from the area D includes the $\{200\}_{L21}$ spots while those are absent from the pattern of the area C. Furthermore, the reverse FFT (RFFT) image constructed from the superlattice $\{200\}_{L21}$ spots shows an inhomogeneous structure with size of several nanometer as shown in Fig. 4(e). These results mean that the fine dark particles observed in Fig. 3(b) have the disordered bcc structure which is the same as the larger particles in Fig. 3(b). The reason why these two different types of the bcc particles exist in this specimen is not clear, but the smaller ones seem to be formed during cooling after the final annealing at least, because of their extremely small particle size. It is very difficult to individually determine the chemical compositions of the precipitate and matrix phases. As mentioned above, the precipitation of the disordered bcc phase in the ordered bcc matrix has already been reported in the Co_2CrAl alloy, where the Cr-rich bcc particles precipitate in the CoAl-rich B2 matrix phase.^{21,22} From analogy with the Co_2CrAl alloy, it is deduced that the precipitation particles have a V-rich composition and that the composition of the matrix $L2_1$ phase deviates from the stoichiometric one to the CoAl-rich direction. This compositional deviation of the matrix $L2_1$ phase may bring about the discrepancy between the experimental and calculated patterns in the XRD.

B. Magnetic properties

Figure 5 shows the magnetization curve measured at 5 K for Co_2VGa at ambient pressure. As seen in Fig. 5, the magnetization curve is characteristic for ferromagnets. The magnetization M at 5 K is saturated in the magnetic field at about 10 kOe, indicating that the magnetocrystalline anisotropy energy of Co_2VGa is small. The spontaneous magnetization was determined by the linear extrapolation to $H/M=0$ of the M^2 versus H/M curve. The magnetic moment was deduced from the value of the spontaneous magnetization at 5 K. The results are $2.04 \mu_B/\text{f.u.}$ and $1.86 \mu_B/\text{f.u.}$ for Co_2VGa and Co_2VAl , respectively. These values are in good agreement with those reported earlier.^{23,24} Note that half-metallic full Heusler alloys follow a Slater-Pauling behavior,¹² i.e., the total spin magnetic moment per formula unit, M_t , in μ_B

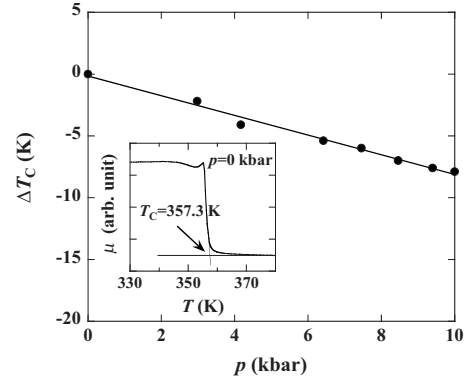


FIG. 6. Pressure shift of the Curie temperature T_C observed for Co_2VGa . Solid line in the figure is a guide for the eyes. The inset shows the initial permeability μ as a function of temperature at ambient pressure for Co_2VGa .

scales with the total number of valence electrons, Z_t , following the rule: $M_t = Z_t - 24$. Namely, the Slater-Pauling behavior predicts that the M_t should be $2.0 \mu_B$ for both Co_2VAl and Co_2VGa . The magnetic moment of Co_2VGa observed in this study is in good agreement with the result expected from the Slater-Pauling behavior. On the other hand, the magnetic moment of Co_2VAl is somewhat smaller than $2.0 \mu_B$, owing to the precipitation of the bcc particles in the matrix $L2_1$ phase as mentioned above. The temperature dependence of M at 0.1 kOe for Co_2VGa is shown in the inset in Fig. 5. We find the considerable thermomagnetic irreversibility on the M versus T curves for the zero-field-cooling (ZFC) and field-cooling (FC) processes. It may be attributed to the pinning of domain walls.

The inset in Fig. 6 shows the initial permeability μ versus T curve for Co_2VGa at ambient pressure. The value of μ decreases rapidly just below T_C with increasing temperature and takes a nearly constant value above T_C . The T_C was defined as the cross point of the linear extrapolation lines from higher and lower temperature ranges on the μ versus T curve, as shown in the figure. The T_C of Co_2VGa is 357.3 K, which is in good agreement with those reported earlier.^{19,23} Similar μ versus T curves for Co_2VGa were observed at various pressures. As shown in Fig. 6, the pressure change in T_C , ΔT_C , for Co_2VGa decreases linearly with increasing pressure. The value of dT_C/dp for Co_2VGa is estimated to be -0.78 K/kbar . The negative pressure dependence of T_C found in Co_2VGa contrasts fairly with that of other Heusler alloys containing Mn atoms,⁴⁻¹⁰ in which T_C increases linearly with increasing pressure. The T_C observed at ambient pressure for Co_2VAl is 342.7 K, which is somewhat higher than those reported earlier.^{19,20,23}

Figures 7(a) and 7(b) show the magnetization curves of Co_2VGa and Co_2VAl , respectively, measured in magnetic fields up to 70 kOe at 5 K under two different pressures. It is seen that the two curves obtained under different pressure are perfectly overlapped in the Co_2VGa , although being apparently different in the Co_2VAl . The magnetic moments per formula unit, μ_s , under various pressures are estimated by using the values of the spontaneous magnetization measured at 5 K. As seen in the inset of Fig. 7(a), the magnetic mo-

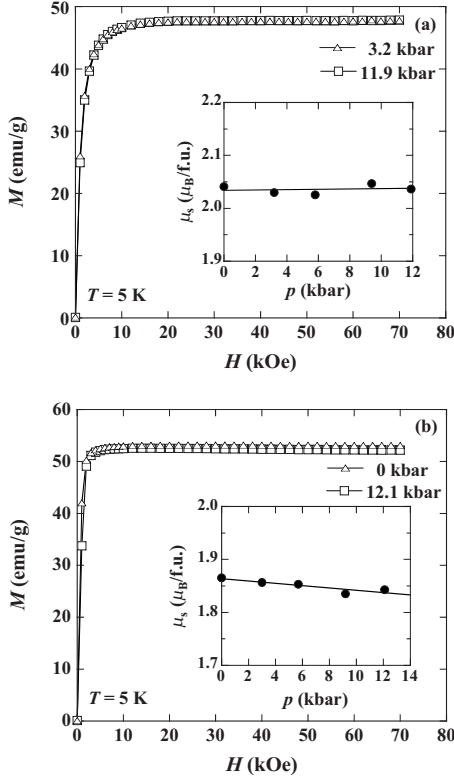


FIG. 7. Magnetization curves measured at 5 K for (a) Co_2VGa (3.2 and 11.9 kbar) and (b) Co_2VAl (0 and 12.1 kbar). The insets in the figures show the pressure dependence of the magnetic moment per formula unit μ_s . Solid lines in the insets are a guide for the eyes.

ment of Co_2VGa is almost independent of pressure. The value of high field susceptibility, χ_h , at each pressure is negligibly small. On the other hand, as shown in Fig. 7(b), the μ_s for Co_2VAl decreases linearly with increasing pressure. The inset in Fig. 7(b) shows the pressure dependence of μ_s at 5 K for Co_2VAl . The pressure derivative of μ_s is estimated to be $-2.2 \times 10^{-3} \mu_B/\text{f.u. kbar}$. It should be noted that the value of pressure derivative of μ_s for Co_2VAl is comparable with that ($= -1.8 \times 10^{-3} \mu_B/\text{f.u. kbar}$) at 5 K for Co_2ZrAl , which is a typical itinerant electron ferromagnet.²⁵

C. Theoretical results

We investigated the pressure effect on the electronic and magnetic properties of Co_2VAl and Co_2VGa theoretically on the basis of first-principles density-functional calculations by using the projector augmented wave method^{26,27} implemented in Vienna *ab initio* simulation package (VASP).^{28,29} We adopt the generalized gradient approximation for exchange-correlation potentials. First, we calculated the total energy of each material in the ordered $L2_1$ structure as a function of the lattice constant. The results for Co_2VAl and Co_2VGa are shown in Figs. 8(a) and 8(b), respectively. The lattice constant and the bulk modulus in the equilibrium condition thus determined are listed in Table I. Both materials possess similar elastic properties with each other as expected from their isostructural and isoelectronic relationship.

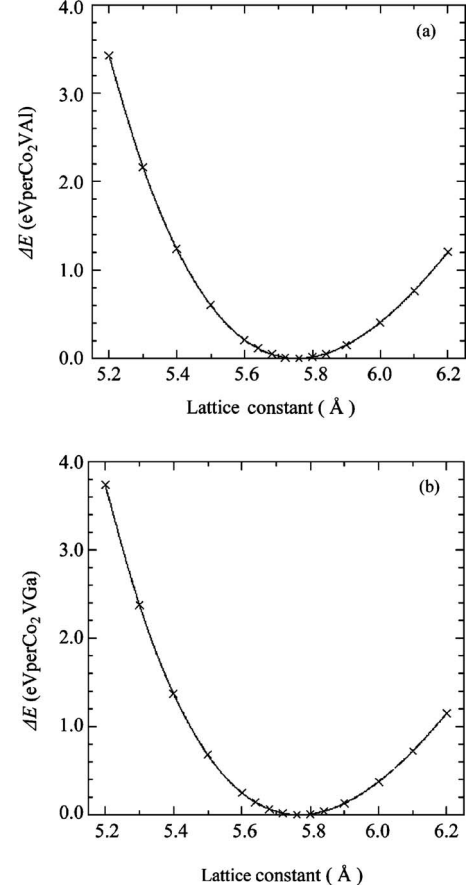


FIG. 8. Total energy relative to the equilibrium value calculated as a function of the lattice constant in the ordered $L2_1$ structure for (a) Co_2VAl and (b) Co_2VGa .

Figures 9(a) and 9(b) show the total, Co, and V magnetic moments calculated for Co_2VAl and Co_2VGa , respectively, as a function of the lattice constant. The total magnetic moment per formula unit at the equilibrium is about $2.0 \mu_B$, which is predicted by the Slater-Pauling rule,¹² for both materials and is almost independent of the lattice constant in the region between 5.6 and 6.2 Å. The result is a direct consequence of half-metallic electronic structure of these materials, i.e., the total magnetic moment remains the same unless the minority-spin energy gap is filled by broadened valence and/or conduction bands. It is noted that the Co and V magnetic moments show the opposite dependence on the lattice constant with each other. While the Co magnetic moment decreases, the V moment increases with decreasing the lat-

TABLE I. The lattice constant, a_0 , and the bulk modulus, B_0 , at ambient pressure calculated for Co_2VAl and Co_2VGa . The experimental data measured in this work are listed in parentheses for comparison.

Material	a_0 (Å)	B_0 (kbar)
Co_2VAl	5.756 (5.7798)	1930
Co_2VGa	5.766 (5.7920)	1980

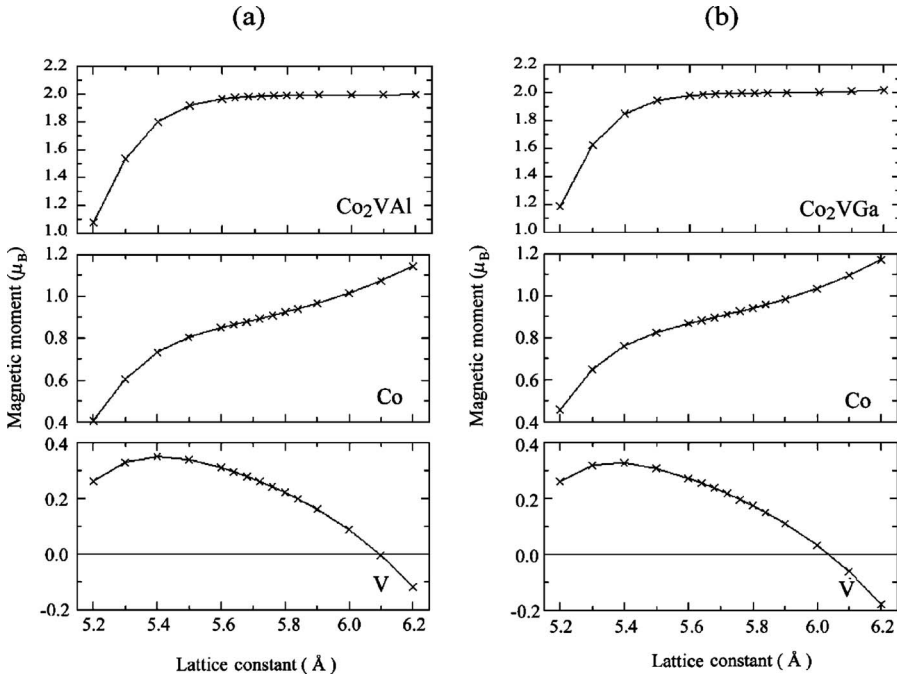


FIG. 9. Total (top panel), Co (middle), and V (bottom) magnetic moments calculated as a function of the lattice constant in the ordered $L2_1$ structure for (a) Co_2VAI and (b) Co_2VGa .

tice constant at around the equilibrium for both materials. The compensation behavior of the pressure dependence of the magnetic moment at each constituent atomic sites has been observed also in other half-metallic Heusler alloys, Co_2MnZ ($Z=\text{Si}$, Ge , and Sn).³⁰ In these materials, however, the Co (Mn) magnetic moment increases (decreases) with decreasing the lattice constant contrary to the behavior in Co_2VAI and Co_2VGa .

With use of the equation of state for each material, we evaluate the derivative of the magnetic moment with respect to pressure. The theoretical result is consistent with the negligible pressure dependence observed experimentally in Co_2VGa whereas it is inconsistent with the experimental observation in Co_2VAI . The discrepancy between the theoretical and experimental results is apparently attributed to the phase separation between the ordered $L2_1$ and disordered bcc phases found only in the Co_2VAI sample. The deviation of stoichiometric composition in the matrix $L2_1$ phase for Co_2VAI sample leads to the degradation of half-metallicity. In particular, the antisite Co defects in half-metallic Heusler alloys give rise to additional electronic states at the Fermi level in the minority-spin energy gap, as confirmed by first-principles calculations for Co_2MnSi , Co_2MnGe , Co_2CrAl , and so on.^{31,32}

IV. CONCLUSION

We have carried out the magnetization measurements at high pressure up to 12.1 kbar for Co_2VAI and Co_2VGa with

a miniature high-pressure clamp cell. We found that the magnetic moment measured at 5 K is independent of pressure for Co_2VGa . This is an experimental observation that gives clear evidence that Co_2VGa possesses half-metallic electronic structure. On the other hand, we observed the sizable pressure dependence of the magnetic moment, i.e., $d\mu_s/dp = -2.2 \times 10^{-3} \mu_B/\text{f.u. kbar}$, for Co_2VAI contrary to the absence of pressure dependence expected generally for HMFs. The discrepancy between the theoretical and experimental results is apparently attributed to the phase separation between the ordered $L2_1$ and disordered bcc phases found only in the Co_2VAI sample. The derivative of the Curie temperature with respect to pressure is -0.78 K/kbar for Co_2VGa , reflecting characteristics typical for usual itinerant electron systems. The negative pressure dependence of the Curie temperature found in Co_2VGa contrasts fairly with that of other Heusler alloys containing Mn atoms.⁴⁻¹⁰

ACKNOWLEDGMENTS

The authors would like to thank H. Yoshida at Institute for Materials Research, Tohoku University for the technical support. This work was partly supported by a grant based on the High-Tech Research Center Program for private universities from the Ministry of Education, Culture, Sports, Science and Technology (MEXT), Japan, and also by a Cooperative Research Project Program of RIEC, Tohoku University. This was also partly supported by a Grant-in-Aid for Scientific Research (Grants No. 19048002 and No. 21560693) from the Japan Society for the Promotion of Science (JSPS)/MEXT.

*kanomata@tjcc.tohoku-gakuin.ac.jp

- ¹G. A. Prinz, *Science* **282**, 1660 (1998).
- ²P. Entel, V. D. Buchelnikov, V. V. Khovailo, A. T. Zayak, W. A. Adeagbo, M. E. Gruner, H. C. Herper, and E. F. Wassermann, *J. Phys. D: Appl. Phys.* **39**, 865 (2006).
- ³A. Planes, L. Mañosa, and M. Acet, *J. Phys.: Condens. Matter* **21**, 233201 (2009).
- ⁴T. Kanomata, K. Shirakawa, and T. Kaneko, *J. Magn. Magn. Mater.* **65**, 76 (1987).
- ⁵K. Shirakawa, T. Kanomata, and T. Kaneko, *J. Magn. Magn. Mater.* **70**, 421 (1987).
- ⁶V. V. Kokorin, S. V. Cherepov, and V. A. Chernenko, *Phys. Met. Metallogr.* **63**, 177 (1987).
- ⁷V. V. Kokorin, I. A. Osipenko, and T. V. Shirina, *Phys. Met. Metallogr.* **67**, 173 (1989).
- ⁸S. Kyuji, S. Endo, T. Kanomata, and F. Ono, *Physica B* **237-238**, 523 (1997).
- ⁹Y. Adachi, H. Morita, T. Kanomata, A. Sato, H. Yoshida, T. Kaneko, and H. Nishihara, *J. Alloys Compd.* **383**, 37 (2004).
- ¹⁰J. Kim, T. Taniguchi, T. Fukuda, and T. Kakeshita, *Mater. Trans.* **46**, 1928 (2005).
- ¹¹E. Şaşıoğlu, L. M. Sandratskii, and P. Bruno, *Phys. Rev. B* **71**, 214412 (2005).
- ¹²I. Galanakis, P. H. Dederichs, and N. Papanikolaou, *Phys. Rev. B* **66**, 174429 (2002).
- ¹³Y. Miura, M. Shirai, and K. Nagao, *J. Appl. Phys.* **99**, 08J112 (2006).
- ¹⁴S. E. Kulkova, S. V. Ereemeev, T. Kakeshita, S. S. Kulkov, and G. E. Rudenski, *Mater. Trans.* **47**, 599 (2006).
- ¹⁵J. Kübler, G. H. Fecher, and C. Felser, *Phys. Rev. B* **76**, 024414 (2007).
- ¹⁶H. C. Kandpal, G. H. Fecher, and C. Felser, *J. Phys. D: Appl. Phys.* **40**, 1507 (2007).
- ¹⁷R. Y. Umetsu, K. Kobayashi, A. Fujita, R. Kainuma, K. Ishida, K. Fukamichi, and A. Sakuma, *Phys. Rev. B* **77**, 104422 (2008).
- ¹⁸R. Y. Umetsu, K. Kobayashi, R. Kainuma, Y. Yamaguchi, K. Ohoyama, A. Sakuma, and K. Ishida, *J. Alloys Compd.* **499**, 1 (2010).
- ¹⁹K. R. A. Ziebeck and P. J. Webster, *J. Phys. Chem. Solids* **35**, 1 (1974).
- ²⁰E. I. Shreder, M. M. Kirillova, and V. P. Dyakina, *Phys. Met. Metallogr.* **90**, 362 (2000).
- ²¹K. Kobayashi, R. Y. Umetsu, R. Kainuma, K. Ishida, T. Oyama, A. Fujita, and K. Fukamichi, *Appl. Phys. Lett.* **85**, 4684 (2004).
- ²²S. V. Karthik, A. Rajanikanth, Y. K. Takahashi, T. Ohkubo, and K. Hono, *Acta Mater.* **55**, 3867 (2007).
- ²³K. H. J. Buschow and P. G. van Engen, *J. Magn. Magn. Mater.* **25**, 90 (1981).
- ²⁴K. Yoshimura, A. Miyazaki, R. Vijayaraghavan, and Y. Nakamura, *J. Magn. Magn. Mater.* **53**, 189 (1985).
- ²⁵T. Kanomata, T. Sasaki, H. Nishihara, H. Yoshida, T. Kaneko, S. Hane, T. Goto, N. Takeishi, and S. Ishida, *J. Alloys Compd.* **393**, 26 (2005).
- ²⁶P. E. Blöchl, *Phys. Rev. B* **50**, 17953 (1994).
- ²⁷G. Kresse and D. Joubert, *Phys. Rev. B* **59**, 1758 (1999).
- ²⁸G. Kresse and J. Hafner, *Phys. Rev. B* **47**, 558 (1993).
- ²⁹G. Kresse and J. Furthmüller, *Comput. Mater. Sci.* **6**, 15 (1996); *Phys. Rev. B* **54**, 11169 (1996).
- ³⁰S. Picozzi, A. Continenza, and A. J. Freeman, *Phys. Rev. B* **66**, 094421 (2002).
- ³¹S. Picozzi, A. Continenza, and A. J. Freeman, *Phys. Rev. B* **69**, 094423 (2004).
- ³²Y. Miura, K. Nagao, and M. Shirai, *Phys. Rev. B* **69**, 144413 (2004).